European Polymer Journal 44 (2008) 3122–3132

Contents lists available at ScienceDirect

European Polymer Journal

journal homepage: www.elsevier.com/locate/europolj

MACROMOLECULAR NANOTECHNOLOGY

Macromolecular Nanotechnology

Elastomer/LDH nanocomposites: Synthesis and studies on nanoparticle dispersion, mechanical properties and interfacial adhesion

S. Pradhan [a,b], F.R. Costa [a,*], U. Wagenknecht [a], D. Jehnichen [a], A.K. Bhowmick [b], G. Heinrich [a]

[a] Leibniz-Institut für Polymerforschung Dresden e.V., Hohe Strasse 6, 01069 Dresden, Germany
[b] Rubber Technology Centre, Indian Institute of Technology, Kharagpur 721 302, India

ARTICLE INFO

Article history:
Received 22 April 2008
Received in revised form 11 July 2008
Accepted 17 July 2008
Available online 25 July 2008

Keywords:
Layered double hydroxide
Nanocomposites
Nanofillers
Modified Mooney–Rivlin equation

ABSTRACT

Layered double hydroxides (LDHs) based elastomer nanocomposites have been synthesized and characterized in terms of nanoparticle dispersion, mechanical properties and interfacial adhesion. Since LDH has basic hydroxyl groups on its surface, its potential as reinforcing filler in elastomers and in additionally a crosslinking agent in carboxylated elastomers has been investigated in details. For this purpose, two different elastomers having widely different polarities and functional groups (e.g., ethylene propylene diene terpolymer, i.e. EPDM and carboxylated nitrile rubber, i.e. XNBR) have been used as the matrix. The pristine LDH based on Mg and Al was modified with decane sulfonate by the regeneration method. The morphological analysis of the nanocomposites (done by X-ray diffraction analysis and electron microscopy) shows that in both matrices LDH particles are dispersed in three different forms, i.e. as primary particles, as exfoliated layers and as soft clusters formed by both of them. However, their relative proportion differs drastically in the two matrices. We have shown in this study that the LDH can significantly improve the mechanical properties in both the system. In XNBR/LDH nanocomposites containing no conventional metal oxide curative, this improvement is very prominent due to secondary interaction between LDH and XNBR matrix indicating that LDH can crosslink carboxalated elastomers. It is also observed that LDH particle promotes strain-induced crystallization in XNBR/LDH. The fracture surface analysis shows that in XNBR/LDH nanocomposite very stable polymer–filler interface is formed and tensile failure takes place through the matrix rather than through the interface. In case of EPDM/LDH nanocomposites the opposite is observed and the polymer matrix hardly wets the surface of the LDH particle.

© 2008 Elsevier Ltd. All rights reserved.

1. Introduction

Layered double hydroxides (LDHs) being layered crystalline materials with easily exchangeable interlayer ionic species have tremendous potential as novel nanofiller for polymers. This has been demonstrated in numerous literatures in recent years, where these anionic clay materials after suitable organic modification have been successfully dispersed in nanoscales in wide ranges of polymer matrices [1–5]. The novelty of LDHs with respect to other competitive materials in this respect includes a great flexibility in choosing organic modifiers (with respect to functional groups, like carboxylates, sulfonates, phosphates, etc.) and various methods of modification process (like, *in situ* synthesis, ion-exchange, regeneration methods, etc.). These advantages provide possibility of modifying LDHs with chemicals having specific functionality, like light/UV stability [6], color and luminescence properties [7], antimicrobial activity [8], etc. Such function integrating hybrid

* Corresponding author. Tel.: +49 351 4658 368; fax: +49 351 4658 290.
E-mail address: costa@ipfdd.de (F.R. Costa).

0014-3057/$ - see front matter © 2008 Elsevier Ltd. All rights reserved.
doi:10.1016/j.eurpolymj.2008.07.025

filler, where the intrinsic functionalities of host (LDH in this case) and guest (modifier) are coupled, can be the next generation hybrid filler to develop polymer composites for advanced applications.

The final properties of a polymer composite filled with inorganic particles always depend on the nature of dispersion of the filler particles and interaction at the polymer–filler interface. In case of polymer/clay nanocomposites, these aspects are more critical as the filler particles have sub-micrometer dimension and large aspect ratio resulting in very high surface area. The homogeneous and stable dispersion of such tiny inorganic particles in an organic matrix is always a challenging task to the material scientists. Because of this large surface area and attractive interaction between the clay layers, strong adhesion at the polymer–filler interface is necessary to obtain a homogenous dispersion of the nanoparticles in the polymer matrix and significant improvement in mechanical properties with a small filler concentration. In the present article, we investigate how the matrix polarity and the presence of reactive functional groups on polymer chain influence the dispersion of nanoclay particles, the polymer–filler interfacial adhesion and the mechanical properties of the elastomer/LDH nanocomposites. Two elastomer matrices widely differing in polarity and chemical nature such as a non-polar elastomer i.e. EPDM (surface energy about 34.0 mJ/m^2) and a polar functionalized elastomer i.e. XNBR (surface energy about 52.0 mJ/m^2) [9] were chosen as the base matrix. Another important aspect that is of special interest here is the presence of chemically active functional group (i.e. –COOH) in XNBR, which may cause some secondary interaction with the hydroxyl groups on LDH particles. The stress–strain behaviors of these nanocomposites have been analyzed using modified Mooney–Rivlin equation to investigate how LDH particles influence the mechanical properties of these two systems.

As nanofiller, LDH differs from layered silicates (the most widely used clay and clay minerals in preparing polymer/clay nanocomposites) in several aspects. LDH has positively charged mixed metal hydroxide layers i.e. $[M^{II}_{1-x}M^{III}_{x}(OH)_2]^{x+}$ stacked one upon another with small anions and water molecules sandwiched in the interlayer region. The general formula of LDH is $[M^{II}_{1-x}M^{III}_{x}(OH)_2]^{x+}(A^{n-})_{x/n}.yH_2O$ where M^{II} is a divalent metal ion, such as Mg^{2+}, Ca^{2+}, Zn^{2+}, etc. M^{III} is a trivalent metal ion, such as Al^{3+}, Cr^{3+}, Fe^{3+}, Co^{3+}, etc. and A^{n-} is an anion, such as Cl^-, CO_3^{2-}, NO_3^-, etc. Though a wide range of values of x is claimed to provide LDH structure, the pure phase of LDH is usually is usually obtained for a limited range as $0.2 \leqslant x \leqslant 0.33$ [10]. However, like layered silicates, the interlayer ions in LDH are exchangeable with large organic species and this makes LDH a suitable precursor for polymer nanocomposite preparation. In the present study, LDH was modified with anionic surfactant namely decane sulfonate by regeneration method. The objective of this organic modification is to enlarge the interlayer distance and make LDH more hydrophobic. For example, modification of LDH by a similar surfactant (dodecyl benzenesulfonate) reduces the surface energy of the material from about 47.7 mJ/m^2 in metal hydroxide to about 27.0 mJ/m^2 in the organo modified LDH [11].

It has already been observed that with addition of organically modified LDH as nanofillers in polymer remarkable improvement in materials properties are obtained in comparison to the pristine polymer or conventional composites [4,12–19]. These improvements include enhanced mechanical properties [4,12], increased heat resistance [13,14], higher photo and UV stability [15,16] and decreased flammability [17–19]. The endothermal decomposition of the metal hydroxide layers in LDHs, is often considered beneficial in improving the flame-retardancy of polymer composites. However, so far majority of polymer/LDH nanocomposites systems reported involves various thermoplastic matrices, like polyolefins, polystyrene, polyamides, etc. No significant study has yet been carried out to investigate the potential of LDHs as nanofiller in elastomer. There are few reports on EPDM/LDH, where nanocomposites have been prepared mostly by solution intercalation method not a conventional technique to process EPDM based composites [20–22]. The melt compounding method still remains unexplored in large extent in preparing elastomer/LDH nanocomposite.

2. Materials and experimental methods

2.1. Materials

EPDM (BUNA EP G 6850, with 60 ± 5 Mooney viscosity ML_{1+4} at 125 °C, density 0.86 g/cc having ethylene content of 51 ± 4 (wt%) and 5-ethylidene-2-norbornene (ENB) as the third monomer (7.7 ± 1.1 wt%) and XNBR containing about 7% carboxylic acid (KRYNAC X 740, with 38 ± 4 Mooney viscosity ML_{1+4} at 100 °C, density 0.99 g/cc) were received from Lanxess, Germany. The Mg–Al layered double hydroxide (PURAL MG 63 HT, Mg:Al = 2:1 approximately) was supplied by the SASOL GmbH, Germany. The anionic surfactant sodium 1-decanesulfonate ($C_{10}H_{21}SO_3Na$) was purchased from Fluka. Sulfur was received from Continental AG, zinc oxide and stearic acid from Acrös Organics, 2-Mercaptobenzothiazole (MBT) from Bayer and tetra methyl thiouram disulfide (TMTD, Vulkacite) from Lanxess.

2.2. Modification of LDH

The pristine LDH was modified using regeneration method as reported earlier [23,24]. The unmodified LDH was first calcined in a muffle furnace for about 4 h at a temperature of 500 °C to convert it into a mixed oxide form (designated as CLDH). The CLDH was then dispersed in an aqueous solution of the sodium-1-decanesulfonate and stirred for about 24 h at 40 °C. The amount of the surfactant in the solution was so maintained that it corresponds to 50% of the anion exchange capacity of the pristine LDH. The modified solid residue was then separated by filtration and dried at 80 °C till constant weight. The modified LDH is henceforth designated as LDH-C10.

2.3. Preparation of elastomer/LDH nanocomposites

The EPDM/LDH and the XNBR/LDH nanocomposites containing different weight percent of LDH-C10 were pre-

pared following a two-step melt compounding method. In the first step, the raw polymer was melted in an internal mixer (HAAKE PolyLab System) at 120° C using a rotor speed of 100 rpm. When constant torque was achieved, desired amount of LDH-C10 was added and further mixed for 7 min under the same conditions. In the second step, all the curatives were added to the elastomer/LDH mix in a two-roll mill (Polymix 110L) at room temperature for approx. 7 min with a friction ratio 1:1:2. Finally, the compounded composites were kept for maturation for 48 h and then vulcanized in a compression molding press at 150 °C temperature and 100 kN pressure. The vulcanization time for each compound was determined from the rheometric study on the uncured samples. The compound formulations for each set of the nanocomposites are given in Table 1. The LDH-C10 content was varied from 5.0 to 10.0 phr. The curative used for both the systems are based on sulfur and accelerators. In case of XNBR/LDH, a small amount of metal oxide curative has been used deliberately to keep the –COOH on XNBR free for possible interaction with LDH-C10 particles.

2.4. Characterization techniques

Wide angle X-ray scattering (WAXS) was performed using 2-circle diffractometer XRD 3003 θ/θ (GE Inspection Technologies /Seifert-FPM, Freiberg) with Cu-K_α radiation ($\lambda = 0.154$ nm) generated at 30 mA and 40 kV in the range of $2\theta = 0.5–25°$ using 0.05° as the step length. The Fourier transform infrared spectra (FTIR) of the LDH materials were obtained using the BRUKER VERTEX 80V spectrometer over the wave number range of 400–4000 cm^{-1}. The powdered samples were mixed with KBR and pressed in the form of pellets for the measurement of FTIR analysis. The Scanning Electron Microscopy (SEM) (microscope model: LEO 435 VP, Carl Zeiss SMT) was used to study morphological features of the powdered samples as well as of the fractured surface of the nanocomposites. The samples were placed on sample holder using conducting carbon cement and then coated with a thin layer of platinum (layer thickness 15 nm) using a sputter coater (BAL-TEC SCD 500 Sputter Coater). The nature of dispersion of the LDH particles in the nanocomposites was also investigated using transmission electron microscopy (TEM) with the microscope TEM JEM 2010. The conditions used during analysis were room temperature, 120 kV acceleration voltage and bright field illumination. The ultra-thin sections of the samples were prepared by ultramicrotomy (Leica Ultracut UCT) at −120 °C with a thickness of a section 100 nm. The dynamic mechanical analysis of the nanocomposites were carried out by DMTA (GABO-EPLEXOR 2000N) within the temperature range of −80 °C to +80 °C at a frequency of 1 Hz and a heating rate of 2 °C/min. Mechanical property of the filled as well as unfilled elastomer/LDH samples were carried out by using ZWICK, Germany.

Table 1
Compound formulations for EPDM/LDH and XNBR/LDH nanocomposites

Ingredient	EPDM/LDH	XNBR/LDH
Elastomer	100	100
LDH-C10 (phr)[a]	X	X
ZnO (phr)	3.0	1.0
Stearic acid (phr)	1.5	1.0
Sulfur (phr)	1.5	0.5
MBT (phr)	1.5	2.0
TMTD (phr)	0.3	–

[a] The value of , X′ varies as 0.0, 5.0, 7.5 and 10.0 phr. Accordingly the EPDM/LDH system is designated as EL0, EL5, EL7.5 and EL10 and the XNBR/LDH system as XL0, XL5, XL7.5 and XL10.

3. Results and discussion

3.1. Characterization of LDH materials

The WAXS patterns of the LDH materials are shown in Fig. 1. It is apparent that both LDH and LDH-C10 are crystalline in nature with well-defined layered structure whereas the calcined form is an amorphous material. The interlayer distance d in LDH and LDH-C10 is obtained from the position of first Bragg's reflection ($\langle 003 \rangle$) using Bragg's equation $n\lambda = 2d\sin\theta$, where n is the order of reflection (equal to 1 for $\langle 003 \rangle$), λ is the wave length of Cu-K_α radiation, and θ is the half of the scattering angle. The modification of LDH with decane sulfonate results in an increase in interlayer distance from 0.76 nm in LDH (corresponding 2θ value of $\langle 003 \rangle$ peak is 11.6°) to 2.27 nm in LDH-C10 ($2\theta = 3.8°$). This increase corresponds to a monolayer arrangement of the decane sulfonate ion in the interlayer region of LDH.

The FTIR spectrum of LDH reveals the presence of interlayer carbonate anion (1367 cm^{-1}) and the broad band in the range of 3200–3700 cm^{-1} shows the presence of water molecules. Due to calcinations of LDH most of the interlayer carbonate ions are lost and the metal hydroxide structure is destroyed, which results in disappearance in characteristic carbonate ion band in the FTIR spectrum of CLDH. Since regeneration of LDH structure in presence of decane sulfonate was carried out at ambient condition, incorporation of some carbonate ion along with decane sulfonate takes place in the interlayer region of LDH-C10. As a result, the 1367 cm^{-1} band reappears after modification. The presence of decane sulfonate in the modified

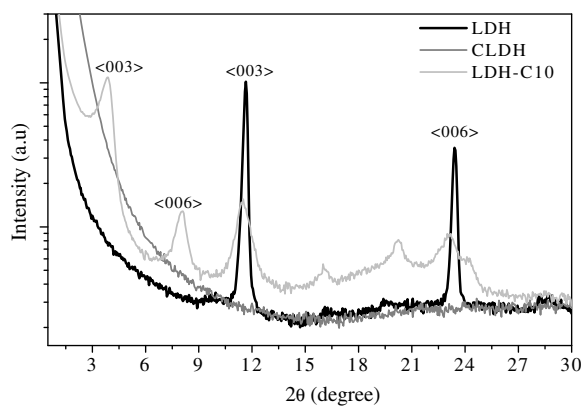

Fig. 1. WAXS patterns of LDH materials: LDH, unmodified form; CLDH, calcined form; LDH-C10, modified form.

LDH is also indicated by strong stretching bands of SO_3 group at 1189 cm^{-1} (asymmetric) and 1049 cm^{-1} (symmetric). The presence of strong stretching bands of the CH_2 units of the hydrocarbon tail of the surfactant can also be observed at 2923 cm^{-1} (asymmetric) and 2852 cm^{-1} (symmetric). The intercalation of alkyl sulfonate within the LDH layers brings about distinct changes in the stretching vibration of the SO_3 group in comparison to its sodium salt form. In the later, the asymmetric stretching vibration of the SO_3 group gives rise to two apparent bands at 1178 cm^{-1} and 1194 cm^{-1} (Fig. 2b) indicating unsymmetrical environment around SO_3 group. In contrast, LDH-C10 show a single sharp and distinct band at 1188 cm^{-1} corresponding to this asymmetric stretching of SO_3 group indicating the equivalent strength and environment of all S–O bonds within the LDH layers [25]. Also the shifting of the symmetric stretching band of the SO_3 group from 1088 cm^{-1} (in the Na salt) to 1049 cm^{-1} (in LDH-C10) is resulted due to such change in the symmetry and bond strength of the SO_3 group.

3.2. Polymer–LDH interaction during melt compounding

The extent of interaction between the EPDM and XNBR matrices and the LDH-C10 particles was monitored with respect to the torque experienced in the mixing rotors of the internal mixer during high temperature melt mixing of the two ingredients. The results are shown in Fig. 3. The interpretations of the torque versus time plots are made from the point of completion of LDH-C10 addition onward. It is obvious that while addition of LDH-C10 in EPDM causes no significant change even after increasing the amount of the filler, a strong increase in the torque can be observed in case of XNBR/LDH with increasing concentration of the filler. It is well known that due to hydrodynamic reinforcement, addition of hard particles in polymeric melt always enhances the modulus. But, in case of EPDM/LDH, this effect is counterbalanced by the plasticizing effect of the surfactant present in the system. Therefore, no noticeable increase in torque can be observed. On the other hand, in case of XNBR/LDH, interaction in addition to the hydrodynamic reinforcement is operative, which surpluses the plasticizing effect of the surfactant resulting in large increases in the torque. The strong polar or even ionic interaction between the polar –CN and acidic –COOH groups of XNBR and basic –OH functionalities on LDH plays a major role in this case. The comparison of the FTIR spectra (Fig. 3c) between the gum XNBR vulcanizates (XL0) and XNBR/LDH nanocomposites reveals that in the later a new band appears at 1583 cm^{-1} corresponding to the C=O stretching vibration of metal carboxylate salt. Though each of the formulations (including XL0) contains small amount of stearic acid and ZnO, this additional band appears only in the XNBR/LDH nanocomposites and its intensity increases as the concentration of LDH is increased. Therefore, this new band is not due to the formation of zinc stearate rather caused by the reaction between the free –COOH groups of XNBR and hydroxyl functionality on the exfoliated LDH particles. Additionally, the intensity of the C=O stretching bands from free –COOH group (1697 cm^{-1} and 1730 cm^{-1}) decreases significantly with increasing LDH concentration, which further emphasizes the decrease of free acid groups with increasing LDH amount.

3.3. Morphological characterization of the nanocomposites

From the X-ray diffraction analysis, the first impression about the nature of dispersion of the LDH particles in both EPDM and XNBR matrix can be made. The WAXS patterns of these two nanocomposites at different LDH concentrations are shown in Fig. 4. The similarity of these patterns between the two systems is that all the first three Bragg's reflections of LDH-C10 can be detected in both. This means that the LDH particles are not fully exfoliated in any of the matrices. However, in EPDM the positions of these reflections do not change by any significant extent from that of LDH-C10 (Fig. 4a). Additionally, these reflections are broad and not well defined. This indicates that LDH particles in EPDM/LDH nanocomposites have highly disordered structure and are characterized by a distribution of interlayer spacing. This can happen when either the LDH-C10

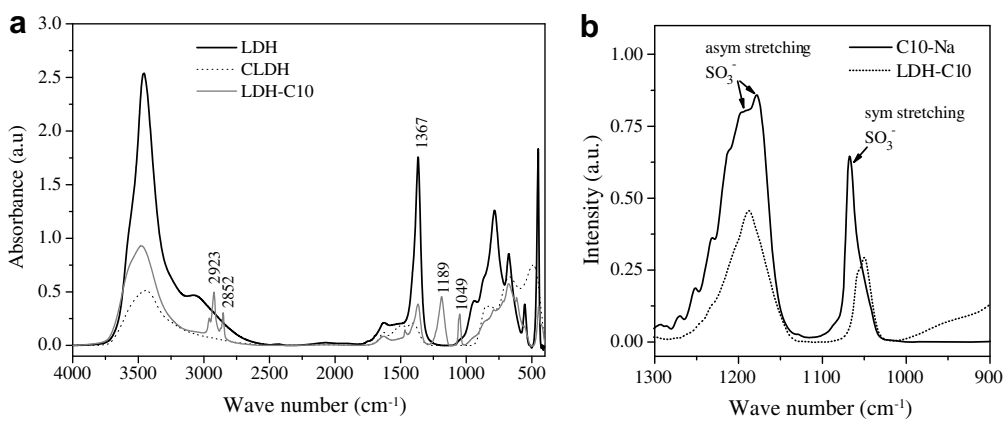

Fig. 2. FTIR spectroscopic analysis of LDH materials: (a) evidence of regeneration of LDH structure after modification (b) evidence of possible interaction between alkyl sulfonate and the LDH layers (C10-Na represents the Na salt of the alkyl sulfonate).

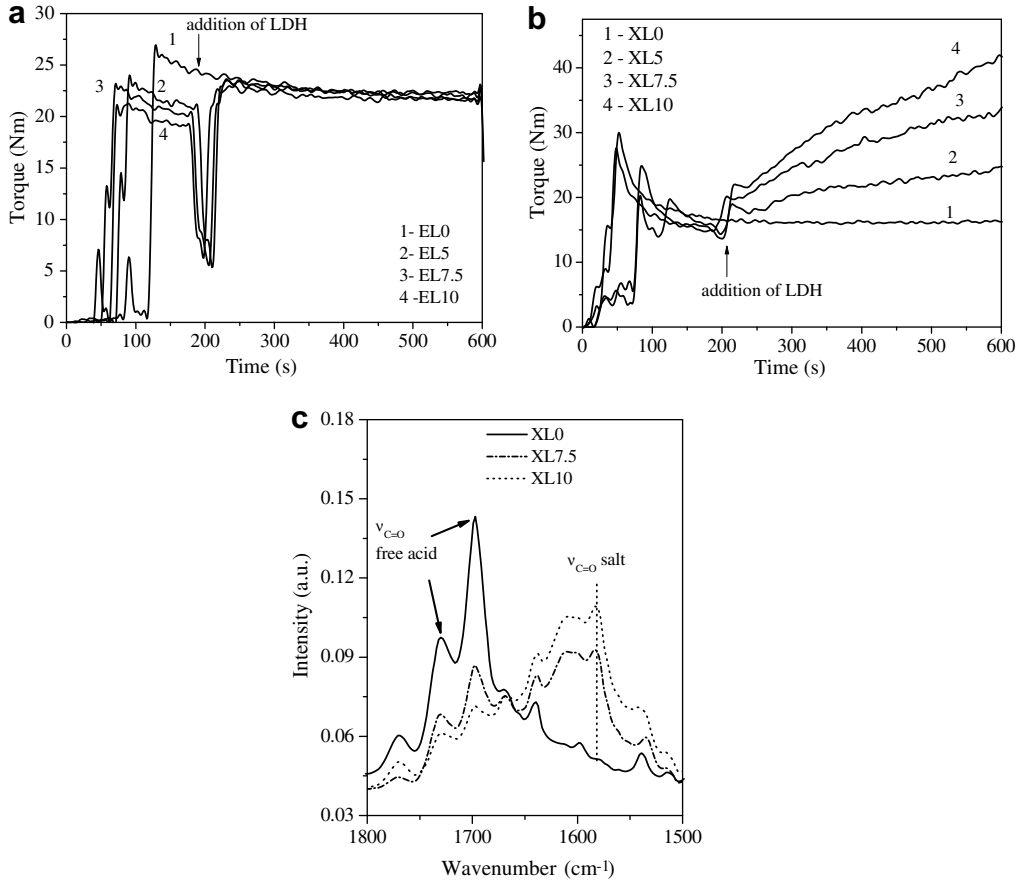

Fig. 3. Analyzing polymer-LDH interactions from the torque vs. time plot during internal mixing of: (a) EPDM/LDH and (b) XNBR/LDH nanocomposites in internal mixer; (c) the FTIR spectra of XNBR/LDH nanocomposites showing possible chemical interaction between XNBR and LDH.

particles loose proper symmetry in crystallographic sense in the direction of stacking of the metal hydroxide layers or EPDM chains intercalate some of the LDH-C10 particles by different extents. On the other hand, The WAXS patterns of XNBR/LDH nanocomposites (Fig. 4b) reveal a distinct evident of intercalation of the polymer chains in the LDH-C10 particles. The shifting of the first Bragg's reflection to a lower scattering angle corresponds to an increase of the interlayer distance by about 0.80 nm. This means multiple number of XNBR chains are aligned within the interlayer space of LDH-C10. Besides, the well-defined Bragg's reflections up to several orders in XNBR/LDH indicate that the LDH-C10 particles have higher crystalline order in spite of the fact that they intercalate multiple numbers of XNBR chains. The exact reason for this difference in crystalline order of the LDH-C10 particles between these two systems is not fully clear to us. The polar/ionic interaction between the functionalities on XNBR and LDH particles might play a major role in easy intercalation of the XNBR chains within LDH-C10 layers without disturbing the crystalline order of the LDH-C10 particles.

The conclusions made from the WAXS patterns of the nanocomposites can be further established by analyzing the TEM micrographs of these materials at various magnifications. These micrographs for both the systems containing 7.5 phr of LDH-C10 are summarized in Fig. 5. It is clear that in these nanocomposites, LDH-C10 particles are dispersed in three different forms: as exfoliated fragments with lateral dimension below 100 nm, as primary particles with lateral dimension from few hundred nm to 1–2 μm and as soft clusters of the primary particles with lateral dimensions over few μm. In case of EPDM/LDH system, the proportions of the last two forms are much higher than the exfoliated fragments, whereas in XNBR/LDH the extent of the exfoliated fragments predominates with less or no cluster formation. The low magnification image of XNBR/LDH (Fig. 5b) shows less number density of the particles compared to that in EPDM/LDH (Fig. 5a). This is due to the fact that in former most of the LDH-C10 particles are exfoliated to the fragments having very fine nanostructured dimensions, which cannot be visualized in low magnification micrographs. However, the higher magnification TEM micrograph of EPDM/LDH nanocomposite (not shown) reveals that the LDH-C10 particles have highly disordered geometry and thus accounts for the broad reflection maxima in the WAXS patterns. In XNBR/LDH the exfoliated LDH particle fragments are homogenously dispersed throughout the matrix and even at this magnification

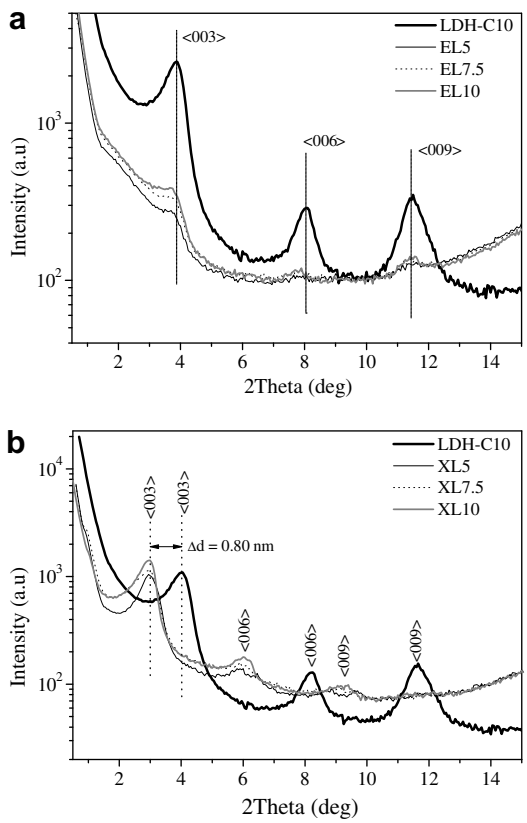

Fig. 4. WAXS patterns of the (a) EPDM/LDH nanocomposites and (b) XNBR/LDH nanocomposites (the number at end of sample designation EL and XL indicates the amount LDH-C10 in phr).

the single LDH layers cannot be distinguished (the thickness of a single LDH layer is 0.48 nm). It seems clear that the polar functional groups on XNBR chains produce strong adhesion at the polymer–filler interface. As a result, the individual metal hydroxide layers in LDH-C10 are peeled off from the surface of the primary particles due to shearing in melt mixing chamber giving a high degree of exfoliation. But, still there exists some unexfoliated LDH-C10 particle, which account for the reflection maxima in the WAXS pattern of this system.

3.4. Dynamic mechanical analysis

Fig. 6 summarizes the DMA results for EPDM/LDH and XNBR/LDH systems. The trends in the variation of the storage modulus with increasing LDH-C10 concentration in the low temperature region (below the glass transition temperature of the respective system) are strikingly different between the two systems. While in XNBR/LDH the storage modulus increases with increasing LDH-C10 amount, in EPDM/LDH it decreases first and then increases. This means that at low LDH-C10 concentration, the EPDM/LDH nanocomposites show a softening effect below glass transition temperature. To explain this behavior the effect of surfactants present in the system should be taken into consideration. LDH-C10 contains large fraction of its weight as anionic surfactant. A part of this surfactant adhered on the outer surface of the LDH particles may be loosely bound and can eventually increase the mobility of the polymer matrix in the polymer–filler interfacial region. This interfacial plasticizing effect can be more influential when the reinforcing effect of the filler particle is low and when small or no secondary interaction occurs

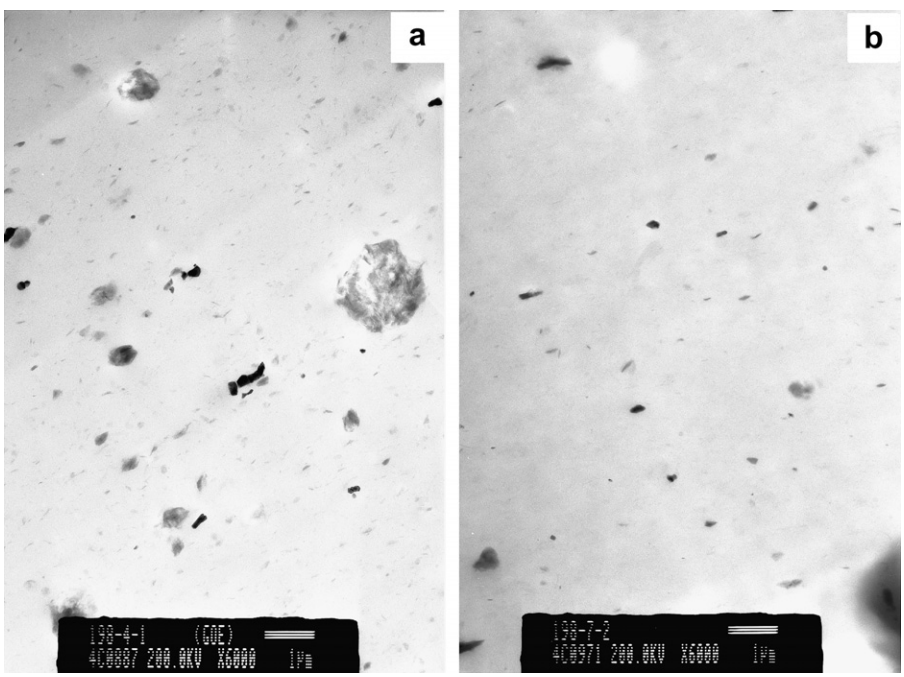

Fig. 5. TEM micrographs of EPDM/LDH (a) and XNBR/LDH (b) nanocomposites with LDH-C10 content of 5 phr (magnification bar 1 μm).

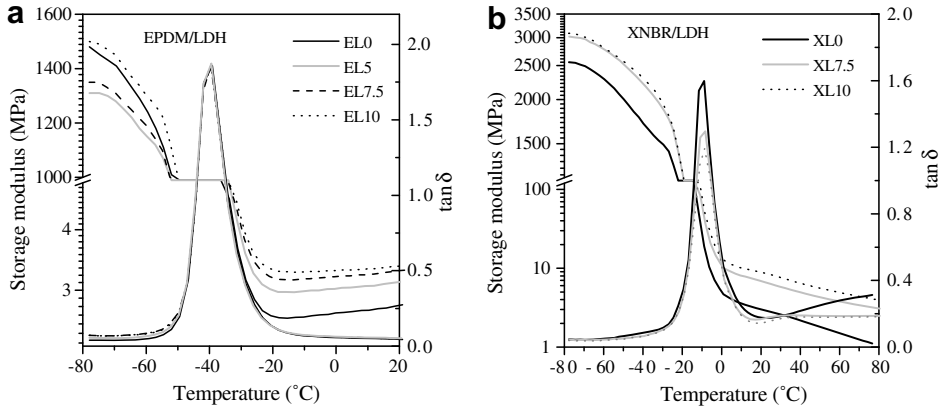

Fig. 6. Dynamic mechanical analyses of EPDM/LDH and XNBR/LDH nanocomposites.

between the polymer and the filler. This is the case with EPDM/LDH nanocomposites, where due to weak interaction at the interface the plasticizing effect dominates at low LDH-C10 concentration resulting in lower storage modulus value at low temperature. However, in case of XNBR/LDH nanocomposites due to strong interfacial interaction between LDH-C10 particles and XNBR matrix, the reinforcing effect dominates in the whole temperature region used in the experiment. At temperature above the glass transition, the segmental movements of the polymer chains become operative and hence the plasticizing effect due to small molecules at the interface becomes less significant. As a result, storage modulus in both the system increases with increasing LDH-C10 concentration.

Fig. 6 also shows the variation of $\tan\delta$ value in the two systems with LDH-C10 concentration. In EPDM/LDH no noticeable change in the maximum of $\tan\delta$ value is observed with increasing LDH-C10 concentration indicating weak or no interaction between EPDM matrix and the dispersed LDH-C10 particles. On the other hand, $\tan\delta$ maximum value steadily decreases with increasing filler concentration in XNBR/LDH showing once again the strong interaction at the interface.

3.5. Mechanical properties

Since EPDM and XNBR matrix interact in different manner with dispersed LDH particles, the influence of LDH concentration on the mechanical properties of these two elastomers will be certainly different. In general, LDH-C10 causes mechanical reinforcement of the both elastomers as the enhancement in tensile strength and modulus can be observed in both cases. The various mechanical properties of these two systems under uniaxial stress are summarized in Table 2 and their typical stress–strain plots are shown in Fig. 7.

Although very low level of curative has been used XNBR based system, the gum vulcanizate shows typical natural rubber like stress–strain behaviour with a sharp upturn in the stress–strain plot after an apparent plateau region (Fig. 7a). This may be a clear indication of strain-induced crystallization. On the other hand, in the EPDM gum vulcanizate stress steadily grows with strain until the material fails. With the addition of LDH-C10 in XNBR matrix, the stress value at all strain increases significantly indicating that the matrix undergoes further curing (Fig. 7b). The upturn in the stress–strain plot becomes more prominent and the plateau region diminishes with increasing LDH-C10 concentration. On the other hand, in EPDM/LDH, the overall nature of the stress–strain plot is not changed much except significant increase in elongation at break and the tensile strength (Fig. 7c). At higher concentration of LDH-C10, a small upturn in the stress–strain plot can also be observed in EPDM/LDH system.

The upturn in the stress–strain plot of elastomers are often attributed to the limitation of extensibility of the

Table 2
Summary of the mechanical properties of EPDM/LDH and XNBR/LDH nanocomposites

Sample	LDH-C10 content (phr)	TS (MPa)	SD	M200 (MPa)	SD	EB (%)	SD
EPDM/LDH							
EL0	0.0	1.54	0.08	0.73	0.01	222	16
EL5	5.0	2.38	0.34	0.78	0.01	390	15
EL7.5	7.5	2.68	0.50	0.84	0.01	420	20
EL10	10.0	3.25	0.35	0.85	0.01	505	34
XNBR/LDH							
XL0	0.0	1.94	0.22	0.41	0.01	1240	59
XL5	5.0	11.96	1.47	1.10	0.01	1220	40
XL7.5	7.5	16.52	1.32	1.31	0.03	1205	36
XL10	10.0	17.83	1.59	1.72	0.08	1047	53

TS, tensile strength; M200, modulus at 200% elongation; EB, elongation at break; SD, standard deviation; phr, parts per hundred rubber.

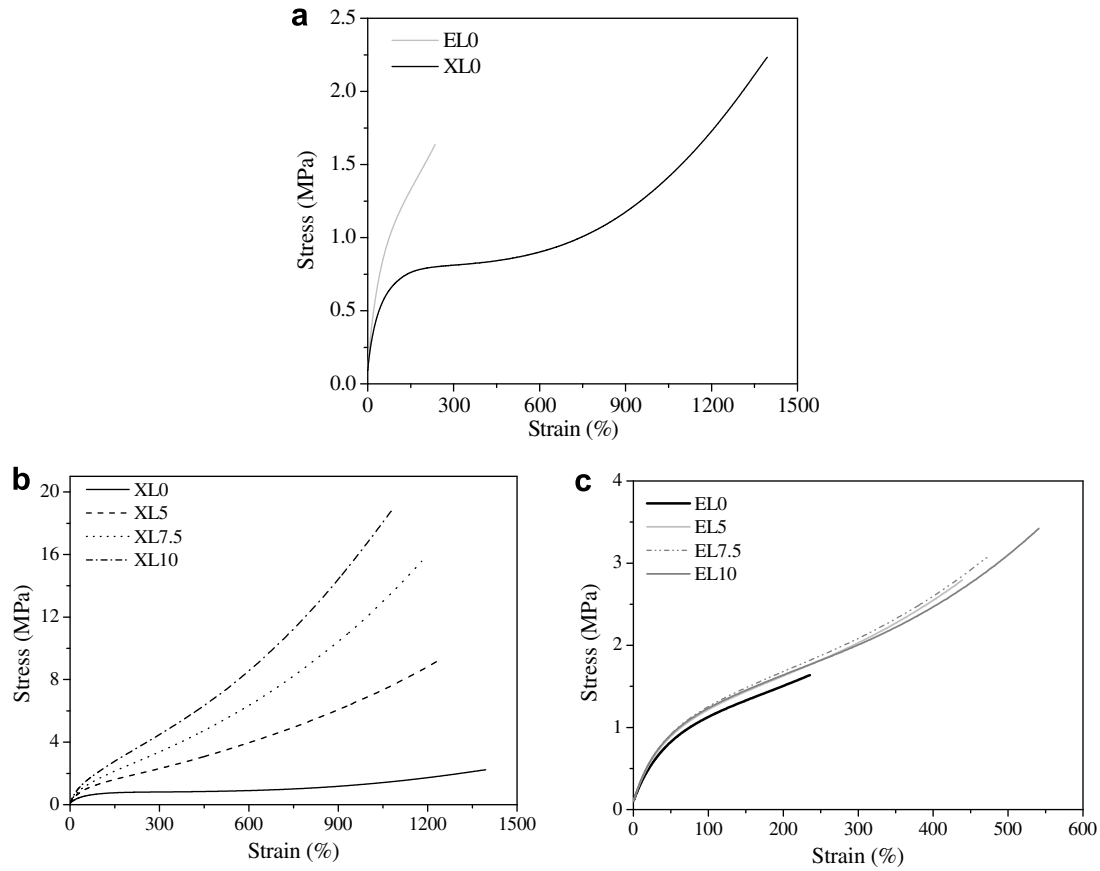

Fig. 7. Typical stress–strain plots of (a) EPDM and XNBR gum vulcanizates, (b) XNBR/LDH and (c) EPDM/LDH nanocomposites.

polymer chains and also to the strain-induced crystallization [26,27]. In original Mooney–Rivlin equation influence these two effects can not be separated. However, the effect of strain-induced crystallization on the stress–strain behaviour of elastomers can be studied using modified Mooney–Rivlin equation proposed by Furukawa et al. where stress–strain relation is derived based on James–Guth's theory and taking into account the chain extensibility factor [28,26]. According to this equation

$$\sigma = 2(C_1 + C_2\alpha^{-1})F(\alpha) \quad (1)$$

where σ is the force divided by the original cross sectional area of the tensile test specimen and C_1, C_2 are the Mooney–Rivlin constants which are independent of the extension ratio α. F(α) is a function of α given by

$$F(\alpha) = \frac{\alpha_m}{2}\ln\frac{1+\alpha/\alpha_m}{1-\alpha/\alpha_m} - \frac{1}{\alpha^2} \quad (2)$$

where α_m is the maximum extension ratio i.e. α at break point in the stress–strain plot. Note, for $\alpha \ll \alpha_m$ the function $F(\alpha)$ approaches the Neo–Hookean stress–strain, which is usually used in the original Mooney–Rivlin equation.

According to equation 1, a plot of $\sigma/F(\alpha)$ against $1/\alpha$ will be a straight line and an upturn at high strain (i.e. low value of $1/\alpha$) is the effect of strain-induced crystallization. The critical value of the strain at which this upturn can be observed is theoretically given by [26]

$$\left(\frac{1}{\alpha}\right)^3_{up} = \frac{2}{3}\frac{1}{\alpha_m^2}\frac{C_1}{C_2} \quad (3)$$

The $\sigma/F(\alpha)$ versus $1/\alpha$ plots (called modified Mooney–Rivlin plot) of EPDM/LDH and XNBR/LDH nanocomposites are shown in Fig. 8 and the calculated values of C_1, C_2 and $1/\alpha_{up}$ are tabulated in Table 3. It is apparent that, the unfilled EPDM and the EPDM/LDH with low concentration of LDH show completely linear relation between $\sigma/F(\alpha)$ and $1/\alpha$ at high strain. The theoretical value of $1/\alpha_{up}$ these materials indicates a strain that is much higher than the strain at the break point in their stress–strain plot. This means the chains rupture before they are sufficiently stressed to a state, where crystallization can be observed. However, in case of EL10, a small upturn in at high strain in Fig. 8a can be observed, indicating a small tendency of strain-induced crystallization. This may be due to the presence of LDH nanoparticles and large content of anionic surfactant at the polymer–filler interface both of which favors orientation of the polymer chains during stressing [29]. The value of C_1 (which depends on the crosslink density and the modulus of the materials) does not change much in EPDM/LDH with increasing LDH concentration indicating low reinforcing effect of LDH-C10 particles on EPDM

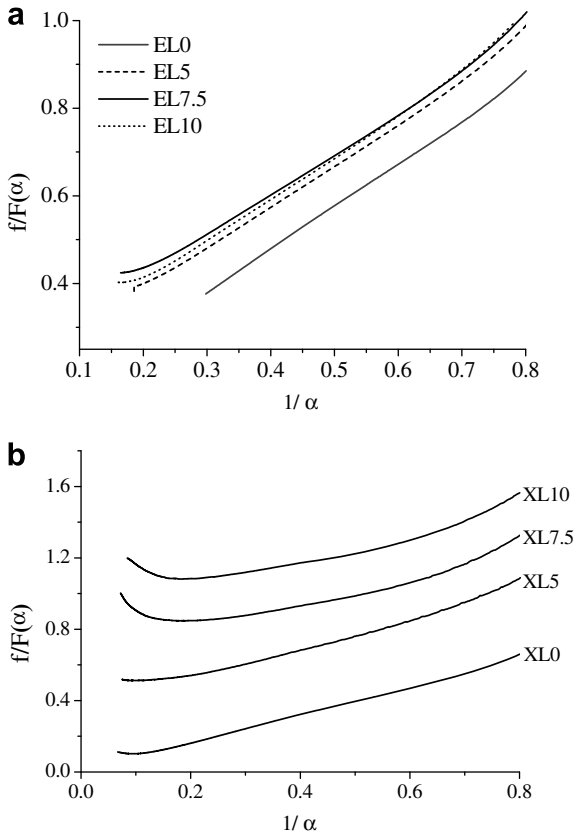

Fig. 8. Stress–strain behavior of EPDM/LDH and XNBR/LDH nanocomposites based on modified Mooney–Rivlin equation.

Table 3
Influence of LDH concentration on the values of C_1 and C_2 with in EPDM/LDH and XNBR/LDH nanocomposites

Sample	C_1 (MPa)	C_2 (MPa)	$(1/\alpha)_{up}$
XNBR/LDH			
XL0	0.004	0.389	0.030
XL5	0.200	0.350	0.129
XL7.5	0.368	0.250	0.172
XL10	0.487	0.250	0.210
EPDM/LDH			
EL0	0.045	0.485	0.176
EL5	0.102	0.463	0.172
EL7.5	0.120	0.452	0.169
EL10	0.112	0.473	0.157

matrix. The small increase in tensile strength and modulus in these materials is simply an effect of the hydrodynamic reinforcement.

In case of unfilled XNBR, a small upturn at high strain in the modified Mooney–Rivlin plot indicates that it undergoes strain-induced crystallization. The crosslink density plays a vital role in determining the extent of this crystallization in the unfilled elastomers [26]. The low crosslink density in case of XL0 (as very small amounts of sulfur curative and metal oxide is added) is the reason for its small extent of strain-induced crystallization and a very low value of $1/\alpha_{up}$ (means a high critical strain). Nonetheless, the addition of LDH-C10 in XNBR causes drastic increase not only in the extent of the upturn in the modified Mooney–Rivlin plot, but also in $1/\alpha_{up}$ value. This means that the LDH-C10 nanoparticles facilitate the strain-induced alignment of the XNBR chains at much lower strain than the unfilled XNBR. A similar phenomenon has also been reported in case of natural rubber/layered silicate nanocomposites [29,30]. It has been suggested that the presence of nanofiller not only accelerates the strain-induced crystallization, but also enhances the extent of strain-induced crystallinity in comparison to the gum compound or the compounds containing conventional fillers, like carbon black and silica. The high degree of exfoliation of the LDH-C10 produces nanoparticles with large aspect ratio and active surface suitable for interaction with the polar functionalities (–CN and –COOH) on XNBR chains. This large interfacial area together with favorable interaction facilitates orientation of the XNBR chains and thus initiates crystallization at much lower strain. The secondary interaction between XNBR and LDH-C10 particles (as demonstrated in Fig. 3) through the chemically active functional groups (–COOH and –OH) leads to the formation of additional crosslinks between the polymer chains through the homogenously dispersed nanostructured LDH particles. As results, the C_1 value sharply increases with increasing LDH-C10 concentration. Additionally, the effect of surfactants (especially those weakly bound to LDH particles) can be very important as they promote higher mobility of the macromolecules at the interface for strain-induced alignment [31].

From Table 3, an interesting difference in the trends of $1/\alpha_{up}$ between EPDM/LDH and XNBR/LDH can be observed. The increase in $1/\alpha_{up}$ value with increasing LDH-C10 concentration in XNBR/LDH is related to the earlier initiation of the strain-induced crystallization. But, in EPDM/LDH, $1/\alpha_{up}$ value shows a slight decreasing trend may be due to the effect of increasing concentration of free or loosely bound surfactant (decanesulfonate). A similar effect has also been observed with increasing concentration of dioctyl phthalate (DOP) (a plasticizer) in case of acrylonitrile butadiene rubber (NBR) vulcanizated filled with DOP [26]. It seems that the presence surfactant molecules enhances the chain extensibility and also facilitates orientation of the EPDM chains under strain. This is further supported by the increasing elongation-at-break with increasing LDH-C10 concentration in Fig. 8b. In case of XNBR/LDH, the effect of the surfactant on the chain extensibility is overtaken by the secondary interaction between XNBR and LDH-C10 particles resulting in lowering of the elongation-at-break in comparison to the unfilled XNBR.

3.6. Fracture surface morphology and the interfacial adhesion

The low magnification SEM images shown in Fig. 9 reveal the overview of fractured surface morphology of the two nanocomposites. It is apparent that the failure of the material follows different mechanisms in the two systems. The EPDM/LDH nanocomposites undergo failure in a single plane without crazing and fibrillation. The formation of microvoids around dispersed LDH particles can be observed (Fig. 9a). This is a clear indication of weak particle–polymer interface, which promotes localized failure at

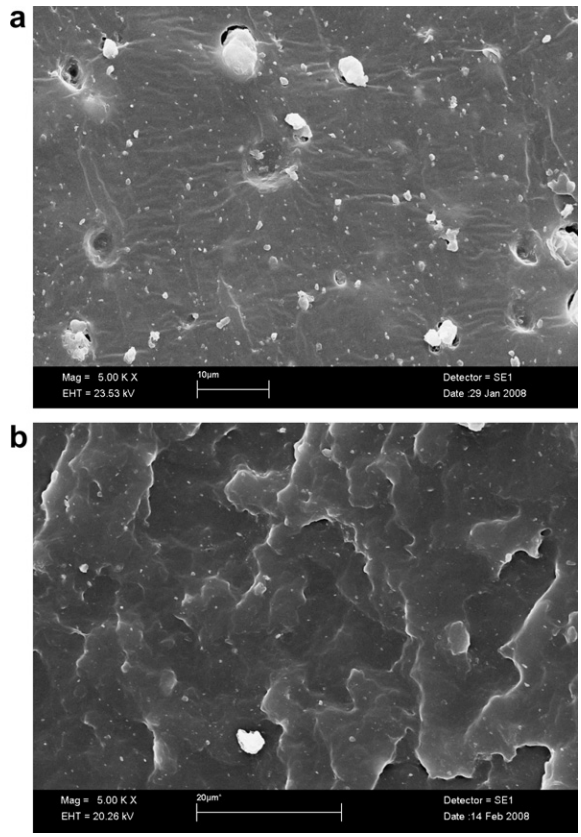

Fig. 9. The fractured surface morphology of EPDM/LDH (a) and XNBR/LDH (b) nanocomposites (LDH-C10 concentration is 10.0 phr) showing the nature of interfacial adhesion between LDH particles and the matrix.

the interface. However, the formation of such isolated microvoids around dispersed nanoparticles gives a mechanism to absorb energy during deformation leading to higher toughness and improved mechanical properties of polymer/clay nanocomposites in comparison to the unfilled polymer [32,33]. Weak polymer–particle adhesion always facilitates interfacial delamination and ultimately the formation microvoids during deformation as can be observed in EPDM/LDH nanocomposites. In contrast, failure of XNBR/LDH nanocomposites is characterized by multiple crazing along different planes with virtually no failure at the particle–polymer interface (Fig. 9b). It seems that when a propagating crack meets LDH particle, it deviates in different directions resulting in multiple failure planes and high roughness on the fractured surface. This is caused by the strong interfacial adhesion between LDH particle and XNBR matrix. Unlike EPDM/LDH nanocomposites, no delamination takes place at XNBR–LDH interface. This is possible only when the dispersed LDH particles form strong bonds with matrix polymer possibly through chemical interaction between –COOH groups of XNBR and –OH groups on LDH particle surface.

4. Conclusion

Layered double hydroxides as nanofiller for polymers have drawn serious attention among researchers in the recent years. We have reported here the preparation and characterization of elastomer/LDH nanocomposites based on two elastomers widely differing polarities and functionalities. The dispersion of the organically modified LDH particles and their interaction with the elastomer matrix were the main aspects highlighted in details. Subsequently, the effect on the mechanical properties of the nanocomposites was investigated. Being anionic clay minerals and having high anion exchange capacity, LDH can be very efficiently modified with anionic surfactants, like alkyl sulfonates. In the present study, the modification of Mg–Al containing LDH with decance sulfonate resulted in large increase in interlayer distance in comparison to the pristine LDH. Although after organic modification LDH become more hydrophobic, it still favors interaction with polymers having polar functionalities. As a result, LDH-C10 particles are more efficiently intercalated and exfoliated in XNBR matrix rather than EPDM giving a homogenous distribution of the primary particles and the exfoliated fragments in XNBR/LDH nanocomposites. On the other hand, in non-polar matrix i.e. EPDM, the LDH-C10 particles are mostly dispersed as primary particles, which also form soft clusters of few μm size. The fractured surface morphology showed that the XNBR matrix nicely wets the LDH-C10 particles whereas EPDM matrix showed poor adhesion with LDH-C10. The differences in the dispersion of the nanoparticles and the interfacial adhesion directly influence the mechanical properties of the nanocomposites. Though in both EPDM and XNBR, LDH-C10 shows reinforcing effect, the changes in mechanical properties in XNBR is much more significant. The polar/ionic interaction between XNBR and LDH-C10 particles is attributed for this difference. Additionally, the LDH-C10 particles influence the typical stress–strain behavior of XNBR, where strain-induced crystallization of the polymer chains is found to accelerate in the presence of LDH-C10 nanoparticles. This study shows that LDH has definite potential as reinforcing nanofiller in elastomer and additionally as curing agent in carboxylated elastomer. This could give rise to possibility of replacing part of conventional metal oxide curative in various functionalized elastomers by organo-LDH. The advantage of using LDH could be the possible function integration through LDH hybrid filler based on modifiers having specific properties, like UV/light stability, antimicrobial activity.

Acknowledgement

S. Pradhan gratefully acknowledges the financial support of the DAAD (German academic exchange service).

References

[1] Leroux F, Besse JP. Polymer interleaved layered double hydroxide: a new emerging class of nanocomposites. Chem Mater 2001;13:3507–15.
[2] Wilson OC, Olorunyolemi T, Jaworski A, Borum L, Young D, Siriwat A, et al. Surface and interfacial properties of polymer-intercalated layered double hydroxide nanocomposites. Appl Clay Sci 1999;15:265–79.
[3] Wang GA, Wang CC, Chen CY. The disorderly exfoliated LDHs/PMMA nanocomposite synthesized by in situ bulk polymerization. Polymer 2005;46:5065–74.

[4] Hsueh HB, Chen CY. Preparation and properties of LDHs/epoxy nanocomposites. Polymer 2003;44:5275–83.
[5] Zammarano M, Bellayer S, Gilman JW, Franceschi M, Beyer FL, Harris RH, et al. Delamination of organo-modified layered double hydroxides in polyamide 6 by melt processing. Polymer 2006;47:652–62.
[6] Perioli L, Ambrogi V, Rossi C, Latterini L, Nocchetti M, Costantino U. Use of anionic clays for photoprotection and sunscreen photostability: Hydrotalcites and phenylbenzimidazole sulfonic acid. J Phys Chem Solids 2006;67:1079–83.
[7] Chang Z, Evans D, Duan X, Boutinaud P, de Roy M, Forano C. Preparation and characterization of rare earth-containing layered double hydroxides. J Phys Chem Solids 2006;67:1054–7.
[8] Li WZ, Li J, Chen JS, Li GD, Jiang YS, Li LS, et al. Phenoxymethylpenicillin-intercalated hydrotalcite as a bacteria inhibitor. J Chem Technol Biotechnol 2006;81:89–93.
[9] Brandrup J, Immergut EH, Grulke EA. Polymer Handbook. Wiley & Sons; 2003.
[10] Cavani F, Trifiro F, Vaccari A. Hydrotalcite-type anionic clays: preparation, properties and applications. Catalysis Today 1991;11:173–301.
[11] Costa FR, Wagenknecht U, Jehnichen D, Heinrich G. Nanocomposites based on polyethylene and Mg–Al layered double hydroxide: characterisation of modified clay, morphological and rheological analysis of nanocomposites. Plastic, Rubber and Composites 2006;35:139–48.
[12] Hsueh HB, Chen CY. Preparation and properties of LDHs/polyimide nanocomposites. Polymer 2003;44:1151–61.
[13] Ding P, Qu B. Structure, thermal stability, and photocrosslinking characterization of HDPE/LDH nanocomposites synthesized by melt-intercalation. J Polym Sci B Polym Phys 2006;44:3165–72.
[14] Costantino U, Gallipoli A, Nocchetti M, Camino G, Bellucci F, Frache A. New nanocomposites constituted of polyethylene and organically modified ZnAl-hydrotalcites. Polym Degrad Stab 2005;90:586–90.
[15] Ding P, Qu B. Synthesis of exfoliated PP/LDH nanocomposites via melt-intercalation: structure, thermal properties, and photo-oxidative behavior in comparison with PP/MMT nanocomposites. Polym Eng Sci 2006;46:1153–9.
[16] Li D, Tuo Z, Evans DG, Duan X. Preparation of 5-benzotrazolyl-4-hydroxy-3-sec-butylbenzenesulfonate anion-intercalated layered double hydroxide and its photostabilizing effect on polypropylene. J Solid State Chem 2006;179:3114–20.
[17] Costa FR, Wagenknecht U, Heinrich G. LDPE/Mg–Al layered double hydroxide nanocomposite: thermal and flammability properties. Polym Degrad Stab 2007;92:1813–23.
[18] Zammarano M, Franceschi M, Bellayer S, Gilman JW, Meriani S. Preparation and flame resistance properties of revolutionary self-extinguishing epoxy nanocomposites based on layered double hydroxides. Polymer 2005;46:9314–28.
[19] Du L, Qu B, Zhang M. Thermal properties and combustion characterization of nylon 6/MgAl-LDH nanocomposites via organic modification and melt intercalation. Polym Degrad Stab 2007;92:497–502.
[20] Acharya H, Srivastava SK, Bhowmick AK. Synthesis of partially exfoliated EPDM/LDH nanocomposites by solution intercalation: structural characterization and properties. Comp Sci Tech 2007;67:2807–16.
[21] Zhang M, Ding P, Du L, Qu B. Structural characterization and related properties of EVA/ZnAl-LDH nanocomposites prepared by melt and solution intercalation. Mater Chem Phys 2008;109:206–11.
[22] Acharya H, Srivastava SK, Bhowmick AK. A solution blending route to ethylene propylene diene terpolymer/layered double hydroxide nanocomposites. Nanoscale Res Lett 2007;2:1–5.
[23] Costa FR, Abdel-Goad M, Wagenknecht U, Heinrich G. Nanocomposites based on polyethylene and Mg–Al layered double hydroxide. I. Synthesis and characterization. Polymer 2005;46:4447–53.
[24] Costa FR, Leuteritz A, Wagenknecht U, Jehnichen D, Häußler L, Heinrich G. Intercalation of Mg–Al layered double hydroxide by anionic surfactants: preparation and characterization. Appl Clay Sci 2008;38:153–64.
[25] Xu ZP, Braterman PS. Competitive intercalation of sulfonates into layered double hydroxides (LDHs): the key role of hydrophobic interactions. J Phys Chem C 2007;111:4021–6.
[26] Furukawa J, Onouchi Y, Inagaki S, Okamoto H. Rubber elasticity at very large elongation. Polym Bull 1981;6:381–7.
[27] Mark JE. Stress–strain isotherms for polymer networks at very high elongations. Polym Eng Sci 1979;19:254–9.
[28] Furukawa J, Okamoto H, Inagaki S. Rubber elasticity at large deformation. Kautschuk u. Gummi Kunststoffe 1976;29:744–50.
[29] Gonzalez JC, Verdejo R, Toki S, Hsiao BS, Giannelis EP, López-Manchado MA. Real-time crystallization of organoclay nanoparticle filled natural rubber under stretching. Macromolecules 2008;41:2295–8.
[30] Joly S, Garnaud G, Ollitrault R, Bokobza L, Mark JE. Organically modified layered silicates as reinforcing fillers for natural rubber. Chem Mat 2002;14:4202–8.
[31] Manias E, Chen H, Krishnamoorti R, Genzer J, Kramer EJ, Giannelis EP. Intercalation kinetics of long polymers in 2 nm confinements. Macromolecules 2000;33:7955–66.
[32] Gloaguen JM, Lefebvre JM. Plastic deformation behaviour of thermoplastic/clay nanocomposites. Polymer 2001;42:5841–7.
[33] Kim GM, Goerlitz S, Michler GH. Deformation mechanism of nylon 6/layered silicate nanocomposites: role of the layered silicate. J Appl Polym Sci 2007;105:38–48.